Journal of Alloys and Compounds 706 (2017) 584–588

Contents lists available at ScienceDirect

Journal of Alloys and Compounds

journal homepage: http://www.elsevier.com/locate/jalcom

Primary and secondary precipitates in a hierarchical-precipitate-strengthened ferritic alloy☆

Gian Song [a, *], Zhiqian Sun [a], Jonathan D. Poplawsky [b], Xiandong Xu [c], Mingwei Chen [c], Peter K. Liaw [a, **]

[a] Department of Materials Science and Engineering, The University of Tennessee, Knoxville, TN, 37996-2200, USA
[b] Center for Nano-phase Materials Sciences, Oak Ridge National Laboratory, Oak Ridge, TN, 37831, USA
[c] World Premier International Advanced Institute for Materials Research, Tohoku University, Sendai, 980-8577, Japan

ARTICLE INFO

Article history:
Received 24 November 2016
Received in revised form
17 January 2017
Accepted 26 February 2017
Available online 27 February 2017

Keywords:
Atom probe tomography
Ferritic steels
Heusler phases
Precipitation
Transmission electron microscopy (TEM)

ABSTRACT

The microstructures of a hierarchical-precipitate-strengthened ferritic alloy are characterized, using transmission-electron microscopy (TEM) and atom-probe tomography (APT). The alloy shows duplex precipitates. The primary precipitate with an average edge length of 90 nm consists of NiAl- and Ni_2TiAl-type phases, while the secondary precipitate with an average radius of 2 nm is a NiAl-type phase. Based on the APT results, the volume fractions of the primary and secondary precipitates were calculated, using the lever rule to be 17.3 and 2.3%, respectively.

1. Introduction

Ferritic steels have been widely employed for high-temperature applications, due to their low cost, high thermal conductivity, and low thermal expansion, as compared to austenitic steels [1–4]. High-Cr ferritic steels are strengthened by nano- and micro-scaled particles, have a small grain size, and contain a high density of dislocations [1,2,5,6]. However, the microstructural instability during the long-term exposure to elevated temperatures, characterized by the coarsening behavior of the precipitate/particle and grain size, as well as a reduction in the dislocation density, restricts their operating temperature to below 900 K [7–9]. There have been extensive efforts to develop creep-resistant ferritic steels with higher temperature capabilities, according to the current US project for the development of ultra-supercritical (USC) steam turbines [10–12], which requires an increase of the steam temperature to 1033 K and the steam pressure to 35 MPa [13].

Along the same lines, the NiAl-precipitate-strengthened ferritic alloys have received recent attention as candidate materials for numerous high-temperature applications, due to their promising creep properties and oxidation resistance [14–16]. Moreover, the structural similarity between the B2-NiAl precipitates and the body-centered-cubic (bcc) Fe matrix leads to the coarsening resistance of the NiAl precipitates during creep deformation [17,18]. However, as the temperature is increased to higher than 923 K, the NiAl-strengthened ferritic alloys exhibit the limited creep resistance, especially at high stresses [19]. The elevated-temperature deformation mechanisms of a NiAl-strengthened ferritic alloy have been investigated, using in-situ neutron-diffraction [20–22], the results of which suggest that the intense diffusion flow along the interfaces between the Fe matrix and NiAl precipitates plays a significant role in affecting the creep deformation [22].

☆ This manuscript has been authored by UT-Battelle, LLC under Contract No. DE-AC05-00OR22725 with the U.S. Department of Energy. The United States Government retains and the publisher, by accepting the article for publication, acknowledges that the United States Government retains a non-exclusive, paid-up, irrevocable, world-wide license to publish or reproduce the published form of this manuscript, or allow others to do so, for United States Government purposes. The Department of Energy will provide public access to these results of federally sponsored research in accordance with the DOE Public Access Plan (http://energy.gov/downloads/doe-public-access-plan).

* Corresponding author.
** Corresponding author.
E-mail addresses: gsong1@vols.utk.edu (G. Song), sunzhiqian2668@gmail.com (Z. Sun), poplawskyjd@ornl.gov (J.D. Poplawsky), xuxiandong000@gmail.com (X. Xu), mwchen@wpi-aimr.tohoku.ac.jp (M. Chen), pliaw@utk.edu (P.K. Liaw).

http://dx.doi.org/10.1016/j.jallcom.2017.02.271
0925-8388/

Recently, we have developed a new ferritic alloy consisting of $L2_1$-Ni_2TiAl precipitates reinforced by narrow B2-NiAl zones, which is referred to as the hierarchical-precipitate-strengthened ferritic alloy and is denoted as HPSFA in the present study [23]. The HPSFA was designed by adding the 2.2 atomic percent (at. %) Ti to a previously-studied NiAl-strengthened ferritic alloy (Fe-12.7Al-10.2Cr-9.0Ni-1.9Mo-0.14Zr-0.024B, at. %, denoted as FBB8 in the present study) [16]. This previous study revealed that the significant improvement in the creep resistance of HPSFA at 973 K was achieved by the presence of the hierarchical precipitates, which formed a coherent interface between the Fe matrix and precipitate phases with optimized elastic strains [23]. Fig. 1 shows the Larson–Miller parameter (LMP) of HPSFA [23], and is compared with FBB8 [24] and conventional steels [P92; Fe-9.09Cr-1.83W, P122; Fe-10.15Cr-1.94W, T122; Fe-10.65Cr-1.87W, and 12CR; Fe-12.1Cr-1.82W in weight percent (wt. %)] [25–28]. More recently, the coarsening behavior of HPSFA has been systematically studied during long-term thermal treatment at 973 K up to 500 h, which reveals the duplex precipitates, such as, the primary and secondary, and the morphological transition of the hierarchical precipitates, which is associated with the elastic coherency of the interface between the primary precipitate and matrix [29]. However, a detailed microstructural characterization of the precipitates is necessary to elucidate the creep mechanism(s) and to achieve the further optimization of the creep properties. Critical precipitate parameters, such as the volume fraction, the composition, and the partitioning behavior of the alloying elements, should be quantified and correlated with the alloy chemistry [30,31].

Thus, the main objective of the current work is to study the microstructures of the HPSFA with a nominal composition of Fe-12.7Al-10.2Cr-9.0Ni-2.2Ti-1.9Mo-0.14Zr-0.024B (in at. %) that exhibits superior creep properties for fossil-fuel power-plant applications. The above-mentioned microstructural features will be determined, using transmission-electron microscopy (TEM) and atom-probe tomography (APT).

2. Method

A plate ingot of HPSFA with a dimension of 12.7 cm × 25.4 cm × 1.9 cm was prepared by the Sophisticated Alloys, Inc., using a vacuum-induction-melting facility. The ingot was hot-isostatically pressed (HIPed) at 1473 K and 100 MPa for 4 h. Chemical analyses were conducted on the ingot to obtain the composition. The alloy was homogenized at 1473 K for 30 min, followed by air cooling, and then aged at 973 K for 100 h. The sharp-tip needle specimens with approximate dimensions of 50–150 nm in diameter and 300–700 nm in length for APT were prepared, using lift-out methods with a FEI Nova focused ion beam (FIB) [32]. The data acquisition was performed, employing a CAMECA local electrode atom probe (LEAP) 4000XHR equipped with an energy-compensated reflectron lens. The APT runs were performed in voltage and laser modes. For the voltage-mode runs, the acquisition parameters were described as follows: 50 K, 200 kHz, 20% pulse fraction, and 0.5% detection rate. For the laser-mode runs, the acquisition parameters were as follows: 30 K, 200 kHz, 25 pJ laser energy, and a 0.5–2.0% detection rate. The TEM samples were prepared in a Zeiss Auriga 40 equipped with a dual electron and FIB. A lamella having dimensions of 12 μm × 6 μm × 1 μm was cut from a heat-treated bulk alloy sample with 30 keV Ga ions. The lamella was lifted out from the bulk sample, transferred to a Cu-grid, and thinned to a thickness of ~100 nm via FIB milling, which was, then, followed by a 5-kV final ion polish to remove the FIB-damaged surface and oxide layer. The TEM was conducted, using a Zeiss Libra 200 MC TEM at an acceleration voltage of 200 kV.

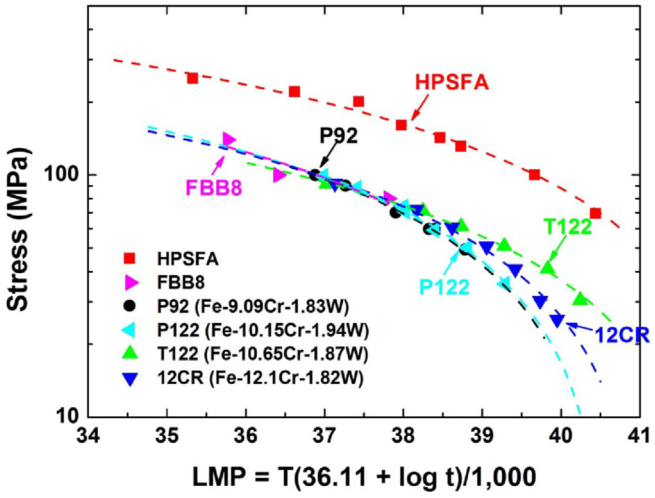

Fig. 1. Larson-Miller parameters (LMP) for HPSFA [24], FBB8 [25], and several conventional steels (P92, P122, T122, and 12CR) [26–29], where the LMP is calculated from T(36.11 + log t)/1000 (T = temperature in Kelvin, and t = time to rupture in hours).

3. Results and discussions

Fig. 2(a)-(b) show the dark-field (DF) TEM images acquired with the specimen oriented along the [110] zone axis using two different reflections in the same region of the sample aged at 973 K for 100 h. The inset in Fig. 2 shows the [110] zone-axis diffraction pattern, where two superlattice reflections were used (marked by red and white circles) to form the DF images. The <111> reflection (a red circle) is unique to the $L2_1$ structure, and, thus, the bright phases in Fig. 2(a) are the $L2_1$ phases. In contrast, when imaged using the <020> reflection (a white circle), which is a common reflection to both $L2_1$ and B2 structures, a slightly-different morphology of the primary precipitate with an average width of 90 nm [23] is observed, as shown in Fig. 2(b). By comparing two images, the B2 and $L2_1$ phases within the precipitate can be differentiated, as marked by white and red arrows, respectively. Specifically, the contrast difference within the precipitate can be observed in Fig. 2(a), which results from the presence of either an anti-phase boundary or another phase in the primary $L2_1$ precipitate, as observed in a similar Fe alloy [33]. Previously, the DF-TEM imaging was used to reveal the formation of the nano-scaled B2 zones in the primary $L2_1$-precipitates [23], and, thus, the narrow zones are likely the B2-type phases.

To verify the TEM results, APT was conducted, the results of which are shown in Fig. 3. Fig. 3(a) shows two iso-concentration surfaces, 10 at. %-Ti and 10 at. %-Ni, which clearly indicate the presence of the B2 and $L2_1$ phases in the precipitates. The compositions of the B2 and $L2_1$ phases derived from the APT analysis are $Ni_{42.8}Al_{38.2}Fe_{14.0}Ti_{4.4}Cr_{0.4}Mo_{0.1}$ and $Ni_{36.2}Al_{29.3}Fe_{18.1}Ti_{15.4}Cr_{0.6}Mo_{0.5}$ in at. %, respectively. A proximity-histogram composition profile between the B2 and $L2_1$ phases is presented in Fig. 3(b), and clearly reveals the Ni, Al, Ti, and Fe partitioning behavior within the primary precipitate. The APT results revealed the formation of secondary nm-size precipitates in the matrix, as was also observed in alloy FBB8 [19]. A 7.6 at. %-(Ni + Ti) iso-concentration surface is shown in Fig. 3(c), which clearly shows the distribution of ultra-fine secondary precipitates in the matrix. The compositions of the matrix, $L2_1$, B2, and secondary precipitates, obtained from the APT results, are summarized in Table 1. Similar duplex precipitates were observed in the NiAl-strengthened ferritic and Ni-based alloys [15,34,35]. Moreover, the microstructural evolution of the HPSFA